ELSEVIER

Contents lists available at ScienceDirect

Water Research

journal homepage: www.elsevier.com/locate/watres





Interactions of graphene oxide with the microbial community of biologically active filters from a water treatment plant

Tanvir Ahamed ^a, Chao Li ^b, Mengyan Li ^b, Lisa Axe ^{a,*}

- ^a Otto H. York Department of Chemical and Materials Engineering, New Jersey Institute of Technology, Newark, NJ, 07102, USA
- b Department of Chemistry and Environmental Science, New Jersey Institute of Technology, Newark, NJ, 07102, USA

ARTICLE INFO

Keywords:
Biological active filters
Graphene oxide
Microbial community
Monod equation
Microbial growth
High-throughput sequencing

ABSTRACT

With widespread occurrence and increasing concern of emerging contaminants (CECs) in source water, biologically active filters (BAF) have been gaining acceptance in water treatment. Both BAFs and graphene oxide (GO) have been shown to be effective in treating CECs. However, studies to date have not addressed interactions between GO and microbial communities in water treatment processes such as BAFs. Therefore, in the present study, we investigated the effect of GO on the properties and microbial growth rate in a BAF system. Synthesized GO was characterized with a number of tools, including scanning electron microscopy (SEM), energy dispersive x-ray spectroscopy (EDX), X-ray diffraction (XRD), Fourier transform infrared spectroscopy (FTIR), and Raman spectrometry. GO exhibited the characteristic surface functional groups (i.e., C-OH, C=O, C-O-C, and COOH), crystalline structure, and sheet-like morphology. To address the potential toxicity of GO on the microbial community, reactive oxygen species (ROS) generation was measured using nitro blue tetrazolium (NBT) assay. Results revealed that during the exponential growth phase, ROS generation was not observed in the presence of GO compared to the control batch. In fact, the adenosine triphosphate (ATP) concentrations increased in the presence of GO (25 μ g/L - 1000 μ g/L) compared to the control without GO. The growth rate in systems with GO exceeded the control by 20 % to 46 %. SEM images showed that GO sheets can form an effective scaffold to promote bacterial adhesion, proliferation, and biofilm formation, demonstrating its biocompatibility. Nextgeneration sequencing (Illumina MiSeq) was used to characterize the BAF microbial community, and highthroughput sequencing analysis confirmed the greater richness and more diverse microbial communities compared to systems without GO. This study is the first to report the effect of GO on the microbial community of BAF from a water treatment plant, which provides new insights into the potential of utilizing a bio-optimized BAF for advanced and sustainable water treatment or reuse strategies.

1. Introduction

Graphene and its derivatives have received significant attention because of their unique properties with respect to thermal conductivity, electron mobility, surface area, and mechanical strength (Andrijanto et al., 2018; Tian et al., 2021). Currently, the most investigated and used form of graphene is graphene oxide (GO), which has been widely applied in numerous fields over the past decade, including environmental engineering, medical devices, electronics, and energy (Dasari et al., 2017; Tian and Wang, 2021; Zou et al., 2016). GO is a 2-D single-atomic layered material made of sp²-bonded carbon atoms with a 0.142 nm bond length (Guerrero et al., 2015). Its honeycomb-like structure includes hydroxyl (C—OH), carboxyl (COOH), carbonyl (C = O), and

epoxy (C—O-C) groups (Zhang et al., 2019). These oxygenated functional groups significantly change the interplane interactions and introduce the hydrophilic character (Hulagabali et al., 2023).

In recent years, GO has been exploited in treating contaminants (Andrijanto et al., 2018; Xing et al., 2020) and as an antibacterial agent to combat drug-resistant bacteria, fouling biofilms, and even fungal pathogens (Anand et al., 2019; Azizi-Lalabadi et al., 2020; Yousefi et al., 2017). For example, Wu et al. (2017) conducted in vitro and in vivo studies revealing that GO exerts inhibitory effects on *K. pneumonia* growth; this, in turn, led to increased survival rates of mammalian lung cells, reduced tissue damage, and mitigated inflammation in various organs. In their study, Wang et al. (2014) successfully developed a ZnO-GO composite, demonstrating bacteriostatic properties against

E-mail address: lisa.b.axe@njit.edu (L. Axe).

^{*} Corresponding author.

E. coli. Furthermore, Grande et al. (2017) found that a GO-chitosan composite film enhanced antibacterial activity, making it more suitable for food packaging applications. On the other hand, over the concentration range of 50 to 500 mg/L, GO was found to support microbial growth in cultures of (pathogenic) bacteria (Guo et al., 2017; Ruiz et al., 2011; Song et al., 2018). More recently, Kumar et al. (2020) effectively degraded microcystin-LR (MC-LR) while removing other contaminants using GO-coated sand co-cultured with Arthorobacter ramosus and Bacillus amyloliquefaciens; these strains are known as potent MC-LR degraders. Other studies have begun to address how GO interacts with microbial communities (Kedves et al., 2020; Lian et al., 2020; Sha et al., 2020). For example, Sha et al. (2020) examined the effects of GO (5-25 mg/L) on the bacterial community in a simulated wastewater treatment process and reported that at 25 mg/L, Firmicutes, Sphingobium, and Leuconostoc showed significantly higher abundance than in control reactors. Furthermore, Sphingobium increased with increasing GO concentrations, while Klebsiella decreased. In another study, Luo et al. (2022) explored the impact of GO concentrations on the bacterial community of rhizospheric soil. Their investigation demonstrated that increasing GO concentrations from 25 mg/L to 500 mg/L led to a change in bacterial community richness; specifically, Actinobacteria, Proteobacteria, Chloroflexi, Acidobacteria, Verrucomicrobia, and Nitrospirae exhibited the greatest increases in abundance. However, interactions between GO and the microbial community in water treatment processes such as biologically active filters (BAF) are still unknown. To better understand how GO contributes to supporting biodegradation rates in water treatment or water reuse, a more systematic study is needed with a microbial community.

BAF in water treatment has been gaining acceptance for treating contaminants of emerging concern (Hess and Morgenroth, 2021; Zearley and Summers, 2012; Zhang et al., 2016, 2017). Granular activated carbon (GAC), with its extensive surface area in the order of 900 m²/g, micro-sized pores, and durable structure, provides a supporting substrate for advancing sustainable biofilms in BAF systems (Zhang et al., 2017). Interestingly, GO, which has demonstrated biocompatibility through interactions with living organisms (Guo et al., 2017; Ruiz et al., 2011; Sha et al., 2020; Song et al., 2018), has a greater specific surface area in aqueous solutions (880-2391 m²/g) (Boulanger et al., 2022; Zhang et al., 2020) than GAC, enabling potentially more interactions between the substrates, contaminants, and microorganisms. Therefore, GO may enhance microbial population growth and stimulate biodegradation in a BAF system. In addition, GO exhibited superior adsorption capacity compared to GAC in treating organic contaminants, including halogenated aliphatic hydrocarbons, polychlorinated biphenyls (PCBs) (Zhou et al., 2015), pesticides (Andrade et al., 2019; Xing et al., 2020), and antibiotics (Gao et al., 2012) in aqueous solutions. Developing a composite by impregnating GO into the GAC surface may improve surface properties, including adsorption capacity and surface area, promoting microbial adhesion and inducing its growth. With limited work available on the impact of GO on biofilm growth and sustainability in GAC-BAF systems, a systematic study is warranted.

In this research, we investigated the effect of GO on the properties and growth of a GAC-based BAF. Specifically, the growth rate of the microbial community in the GAC-BAF is investigated, along with the generation of reactive oxygen species (ROS). We use scanning electron microscopy (SEM) to observe the surface morphology of biofilm before and after exposure to GO to examine the interactions of GO with GAC-BAF samples. Additionally, changes in the microbial community are investigated using Illumina MiSeq 16S rRNA sequence analysis. This research offers valuable insights into the application of a bio-optimized BAF for advanced and sustainable water treatment.

2. Materials and methods

2.1. Synthesis of graphene oxide

All the chemicals used were of reagent grade and purchased from Fisher Scientific. GO was synthesized following the modified Hummer's method (Hummers, 1958). Briefly, graphite powder (140 g/L), K₂S₂O₈ (100 g/L), and P₂O₅ (100 g/L) were heated in an Erlenmeyer flask at 80 °C with concentrated H₂SO₄ for 5 h. Subsequently, the flask was placed in an ice bath and diluted with H₂O (17 % of total volume), which was slowly added to stop the reaction. The solid sample remaining was rinsed several times through vacuum filtration (0.2 μm) and dried overnight. This pretreated graphite powder was then mixed with concentrated H₂SO₄ (50 g/L), KMnO₄ (140 g/L), and NaNO₃ (20 g/L) in the Erlenmeyer flask in an ice bath (at less than 10 °C). After 3 h of reaction, the mixture was sonicated for 10 min, and 1000 ml (67 % by volume) of deionized water (DI) was added slowly. Subsequently, H₂O₂ (40 ml/L) (30 %) was added slowly to the mixture to remove the residual manganese ions that precipitated as MnO₂. The sample was then washed sequentially using 1 M of HCl and DI water and dried for 48 h at room temperature.

2.2. Methods for characterizing GO

The structure and morphology of synthesized GO were characterized by using a number of analyses, including SEM, X-ray diffraction (XRD), Fourier Transform infrared spectroscopy (FTIR), and Raman spectrometry. The surface morphology of GO was evaluated with an SEM JEOL JSM 7900F, operating at 12.0 keV. Before imaging, the GO films were coated with AuPd (~10 nm) to improve conductivity and reduce charging using an EMS Quorum sputterer (Aliyev et al., 2019). Energy dispersive X-ray spectroscopy (EDX) analysis was performed to confirm the weight percentage of oxygen and carbon atoms in the synthesized GO. XRD analysis was performed using a scanning rate of 6° min⁻¹ with a PANalytical EMPYREAN XRD and Cu Kα radiation at voltage 45 kV and current 40 mA. FTIR spectroscopy was carried out using an Agilent Cary 610 spectrometer over 400 to 4000 cm⁻¹. For FTIR, powder samples were prepared using the potassium bromide (KBr) pellet method (Hulagabali et al., 2023). Raman spectroscopy was carried out using a Bruker Scientific DXR Raman microscope (Model: DXR3xi) with a 532 nm wavelength laser and filter.

2.3. GAC-BAF sample collection and source water preparation

The GAC-BAF samples (Calgon Filtrasorb 820; diameter 1.0–1.2 mm) were collected from the Passaic Valley Water Commission (PVWC) in New Jersey. Samples were transported to the laboratory in High-Density Polyethylene containers and maintained at 4 °C. Source water was prepared to simulate the influent water composition of the treatment plant and used as a culture medium for this study (Table SI-1). Preparation of the source water nutrients was adapted from a previous study (Zhang et al., 2017). Briefly, carbon, nitrogen, and phosphorus were added for a mass ratio of 15:5:1, ensuring that these nutrients promoted microbial growth (without limiting any nutrient). A similar C:N:P ratio was applied in other studies focused on drinking water biofilters (Liu et al., 2001; Urfer and Huck, 2001). Sodium phosphate and sodium nitrate were used as phosphorous and nitrogen sources, respectively. Formaldehyde (100 mg/L), glyoxal (30 mg/L), formate (400 mg/L), and acetate (300 mg/L) were added to the simulated source water as carbon sources that resulted in an initial dissolved organic carbon concentration of 7.0 \pm 0.1 mg/L and is consistent with other studies (Liu et al., 2001; Urfer and Huck, 2001; Zhang et al., 2017). These biodegradable compounds were selected because they tend to be generated in the greatest yield as organic by-products from ozonation (Liu et al., 2001; Maeng et al., 2011).

2.4. Method of dosing GO to GAC-BAF sample

The GAC-BAF samples (200 mg/L) were studied in batch reactors run in triplicate, where GO was added in concentrations ranging from 0 to 1000 µg/L from a stock solution of GO that was homogeneously dispersed in DI water (2 mg/L) without producing any agglomeration. The range of concentrations of GO used included 25, 100, 400, 750, and 1000 µg/L. Prior studies demonstrated that GO concentrations in the 25-300 mg/L range promoted microbial community growth in wastewater treatment processes (WWTs) (Kedves et al., 2020; Lian et al., 2020; Wang et al., 2013); however, the viable biomass based on ATP concentration in WWTs (i.e., 2.2 mg ATP/g dry media to 3.7 mg ATP/g dry media) (Jørgensen et al., 1992; Vang et al., 2014) is much greater than that found in water treatment plants $(1.96 \times 10^{-4} \text{ mg ATP/g dry})$ media to 2.8×10^{-3} mg ATP/g dry media) (Magic and Kooij, 2004; Velten et al., 2011; Zhang et al., 2017). Given the ATP concentrations, lower GO concentrations were used in this study and are consistent with the ATP:GO ratios applied in other studies. GAC-BAF samples were incubated in the exponential growth phase up to 48 h, and samples were collected at select incubation times (i.e., 18 h, 24 h, 30 h, and 48 h). This research focused on addressing the potential benefits of GO amendments in a GAC-BAF system to model and scale up. Therefore, reaction kinetics during the exponential growth phase were investigated, and systems with and without GO were compared quantitatively. Specifically, microbial growth parameters, including specific growth rate (μ_{max}), Monod constant (Ks), and biomass yield (Y), were assessed.

2.5. Reactive oxygen species (ROS) generation and oxidative stress

GO-induced oxidative stress has been regarded as the most widely accepted mechanism involved in the antibacterial activity of GO (Gurunathan et al., 2012). The presence of oxidative stress has the potential to disrupt vital cellular functions and interfere with bacterial metabolism, ultimately resulting in the deactivation of bacterial cells. Oxidative stress in cells is a well-established consequence of exposure to ROS. Previous studies have documented concentration-dependent ROS production by GO (Guo et al., 2017; Siqueira et al., 2022; Song et al., 2018). Therefore, the evaluation of ROS production by GO during biofilm formation was assessed using the nitro-blue tetrazolium (NBT) reduction assay (Guo et al., 2017; Pelin et al., 2018). The assay takes advantage of the ability of NBT, a yellow dye, to be reduced to formazan, a blue-purple insoluble compound, in the presence of superoxide radicals. This color change is equivalent to the levels of superoxide production in cells. GAC-BAF samples exposed to GO concentrations (discussed in Section 2.4) were collected after 18 h, 24 h, 30 h, and 48 h, and ROS concentration in the bacterial biofilm was then quantified. Briefly, the GO-exposed GAC-BAF sample was placed in a microcentrifuge tube with 0.5 mL of 1 mg/mL NBT and incubated for 30 min. The insoluble formazan was then extracted with 2 M KOH and dimethyl sulfoxide (96 %) (v/v: 1:3), and the absorbance was recorded at 630 nm under the microplate reader (Guo et al., 2017). The negative control for ROS generation did not include GO, whereas the positive control included 3 mM of H₂O₂ for the oxidation of NBT (Gurunathan et al., 2012). For the positive control, GAC-BAF samples were exposed to H₂O₂ for 45 min and then incubated with NBT for 30 min (Engelbrecht et al., 2024). In this experiment, H₂O₂ was used as a positive control to verify that reduced formazan was produced by superoxide radicals generated when H₂O₂ breaks down, validating the experimental method (Coyle et al., 2006). The results are expressed as % of ROS generation as compared to control without GO.

2.6. Biofilm formation ability of microbes exposed to GO suspensions

Adenosine triphosphate (ATP) is vital in storing energy within cells and is the primary energy currency for all living organisms (Velten et al., 2007). In biofilm studies, ATP analysis has been used to assess the total

biomass of viable cells within a biofilm. Because ATP is present in living cells, increases in ATP concentrations indicate increases in the number of viable cells and, consequently, a more substantial biofilm formation (Zhang et al., 2016). Therefore, ATP concentrations were used to quantify biomass in GO-exposed GAC-BAF samples. GO concentrations applied in the systems (i.e., 25 $\mu g/L$ to 1000 $\mu g/L$) were dosed as described in Section 2.4. The GAC-BAF samples were incubated over 48 h at room temperature with an orbital shaker at 100 rpm. Measurement of ATP was assessed at select incubation times (18 h, 24 h, 30 h, and 48 h) following Velten et al. (2007). Briefly, samples exposed to GO were collected from the reactor, and ATP was extracted using BacTiter-GloTM reagent (1 g/L). The resulting luminescence was measured as relative light units using a luminometer (GloMax®) and converted to an ATP concentration using a calibration curve constructed with a pure ATP standard.

2.7. SEM imaging of GO-exposed GAC-BAF

SEM imaging of biofilms was performed to observe the biofilm features and structure as visible evidence of the interaction of GO with GAC-BAF samples. Briefly, for SEM analysis, at the end of 48 h incubation, samples were collected from each reactor and rinsed three times with sodium cacodylate phosphate buffer (0.1 M, pH = 7.4) (Chen et al., 2014). All samples were serially dehydrated with increasing concentrations of ethanol (20 %, 40 %, 60 %, 80 %, and 100 %) and vacuum dried for 4 h (Dong et al., 2018). Each step has a minimum duration of 20 min, except the last step, during which the GAC-BAF samples are left in pure ethanol overnight (Velten et al., 2007).

2.8. High-throughput Illumina amplicon sequencing and taxonomy analysis

Untreated and GO-treated GAC-BAF samples were used in DNA extraction using PowerSoil® DNA Isolation Kit (MoBio Laboratories, USA) following the manufacturer's instructions (Zhang et al., 2018). Cell disruption and the subsequent extraction of DNA were accomplished through bead-beating techniques. The DNA in the extracts was purified and concentrated using the Genomic DNA Clean & Concentrator Kit (Zymo Research, USA) before measuring its concentration with a Nanodrop spectrophotometer. Polymerase chain reaction (PCR) amplicon libraries for 16S rRNA gene sequences were constructed applying primers 338F (5'-ACTCCTACGGGAGGCAGCA-3') and (5'-GGACTACHVGGGTWTCTAAT-3') (Li et al., 2019b; Zhang et al., 2023; Zhou and Xu, 2020). PCR amplification was performed in Phusion® high-fidelity PCR Master Mix (Thermo Scientific, USA) by initial denaturing at 98 °C for 30 s, then running for 35 cycles of denaturing at 98 °C for 10 s, annealing at 48 °C for 30 s, and extension at 72 °C for 30 s, and a final extension at 72 °C for 10 min (Li et al., 2019a). PCR products were processed by 1 % agarose gel electrophoresis to validate target amplicon bands. After that, target bands were selectively cut and purified using a GeneJET Gel extraction kit (Thermo Scientific, USA) for the following sequencing. Triplicates of PCR products from the same sample were composited to obtain a representative DNA sample, which is consistent with other studies (Forstner et al., 2019; Lian et al., 2020; Sha et al., 2020) as a comprehensive DNA sample improves the detectability, reproducibility, homogeneity, and accuracy in Next-Generation Sequencing (Litchfield et al., 2020). Because of the quality of sequencing data and with no variability in the experimental setup, one representative DNA sample for each GO concentration applied was used for sequencing. Purified DNA amplicons were diluted to 20 $ng/\mu L$ in 25 μL (500 ng) and sent out for amplicon sequencing at Azenta (South Plainfield, NJ, USA). 16S amplicon sequencing data was processed by vsearch (v2.15.2) combined with usearch (v10.0.240) in conda (23.3.1) deployed in linux_x86_64 (Ubuntu 18.04.3 LTS) for primers cutting, quality control (score≥20/fastq_maxee_rate = 0.01), denoise, ASV table and taxonomy annotation (Edgar, 2010; Liu et al., 2021; Rognes et al.,

2016). Taxonomy was annotated against Greengenes2 (v2022.10) for bacterial community analysis (McDonald et al., 2023).

2.9. Statistical analysis

The statistical analysis was conducted using SPSS software. As the data set was small (n < 10), significant differences between experimental results were determined through a non-parametric test, the Sign Test (Nahm, 2016), by comparing the median of independent samples (GO-exposed samples: w/GO₂₅ and w/GO₁₀₀₀) in terms of ROS generation to determine if they significantly differ from the control (w/o GO),

considering statistical significance at a p-value < 0.05.

3. Results and discussion

3.1. Characterization of GO

From the SEM analysis, the structure and surface morphology of the synthesized GO (Fig. 1a) reveal exfoliation into thin nanosheets with the characteristic wrinkled and folded structure. The presence of irregular edges, rough surfaces, and crumpling results from the folding or rolling of two-dimensional GO sheets and indicates that the graphene layers

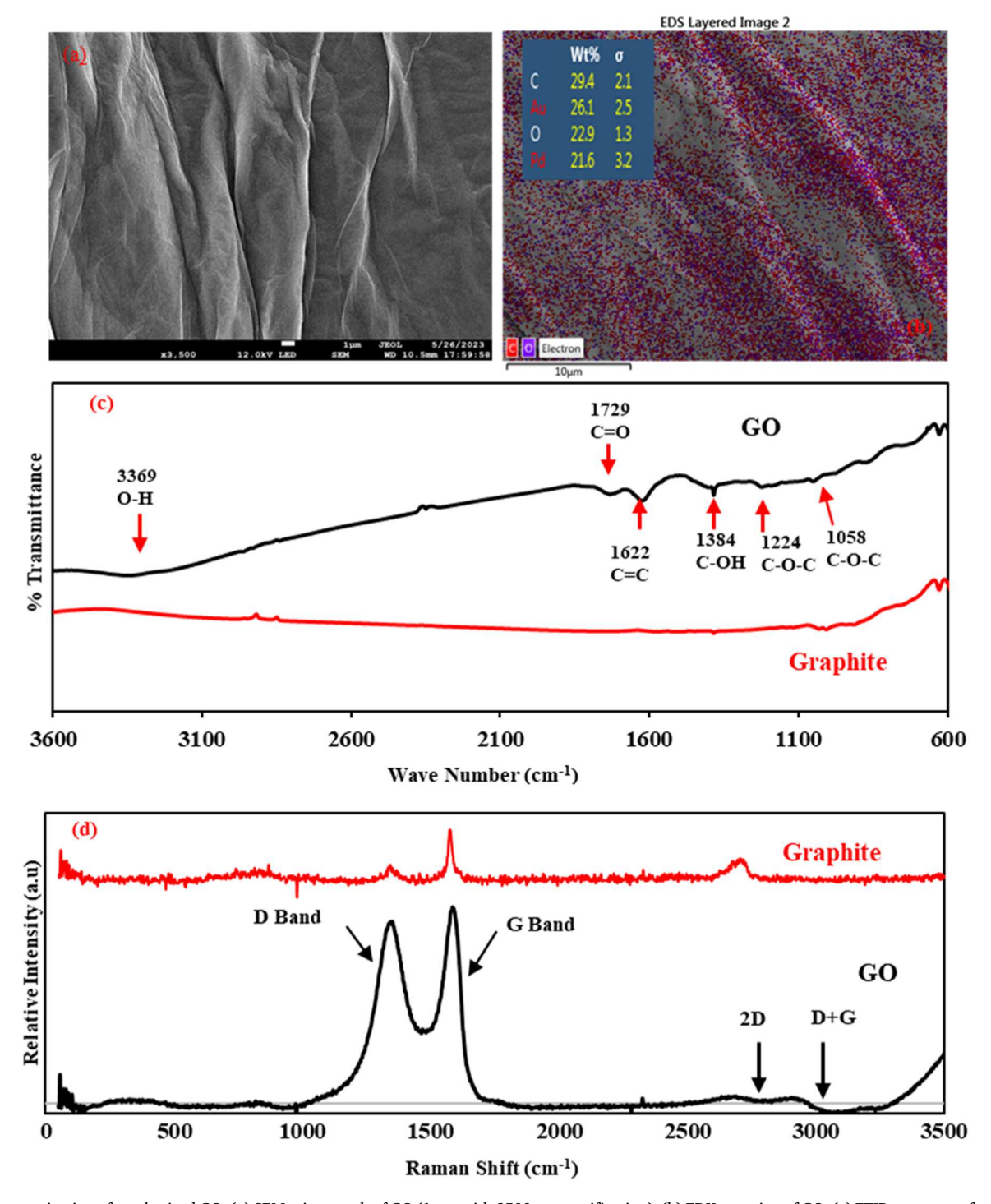


Fig. 1. Characterization of synthesized GO: (a) SEM micrograph of GO (1 μ m with 3500 \times magnification); (b) EDX mapping of GO; (c) FTIR spectrum of graphite and GO; (d) Raman spectra of graphite and GO.

were fully oxidized to GO (Zhang et al., 2019). Other studies (Muniyalakshmi et al., 2020; Neelgund et al., 2013) also confirmed such corrugated and scrolling morphology of GO, which is attributed to the presence of oxygen-containing functional groups on the chemically modified GO sheets. To further assess GO properties, elemental analysis was conducted to determine the C/O ratio in terms of the weight percentages. EDX mapping shows (Fig. 1b) that the majority of the GO is carbon (29.4 % of mass), followed by oxygen (22.9 % of mass) with a C/O ratio of 1.28. This ratio is slightly lower than the ratios (1.43–1.77) reported in other studies (Alam et al., 2017; Guerrero et al., 2015) and confirms that GO samples are oxidized.

The FTIR spectra reveal the presence of oxygenated functional groups on GO surfaces (Fig. 1c). Specifically, a broad peak at 3369 cm⁻¹ confirms the stretching and bending vibration of -OH groups from water molecules adsorbed on the surface (Hidayah et al., 2017). This peak supports the presence of intercalated water and graphene oxidation and demonstrates the improved hydrophilicity of GO. The presence of two absorption peaks at 1622 cm⁻¹ and 1729 cm⁻¹ can be attributed to asymmetric vibrational stretching of sp²- hybridized C=C and C=O of carboxylic acid and carbonyl groups found at the edges of GO (Alam et al., 2017). In addition, the absorption peaks at 1224 cm $^{-1}$ and 1058 cm⁻¹ can be attributed to the stretching vibration of the epoxy groups (C-O-C) (Guerrero et al., 2015). Finally, the absorption peak at 1384 cm⁻¹ denotes O—H deformations in C—OH groups of carboxylic acid (Xing et al., 2020). The FTIR results of the GO are consistent with other studies (Alam et al., 2017; Xing et al., 2020). The initial graphite spectrum did not exhibit any of these peaks. Therefore, these oxygen-containing functional groups are indicative of graphite oxidation.

Raman spectroscopy is a non-destructive technique that is widely used to obtain structural information about carbon-based materials (Alam et al., 2017). The main features of pure graphite are the G and D peaks and their overtones. The two most intense peaks are at 1578 cm^{-1} (G band), corresponding to the tangential stretching (E_{2g}) mode of highly oriented graphite and at 2725 cm⁻¹ (2D band), which represents the disorder in sp² hybridized carbon atoms (lattice distortion) (Alam et al., 2017; Zhang et al., 2019). Another characteristic peak is located at approximately 1363 cm⁻¹ (D band) and relates to the structural defects and partially disordered structures of the sp2 domains. The Raman spectra of GO (Fig. 1d) show the presence of a very strong D peak at about 1363 cm⁻¹ with an intensity comparable to that of the G peak at approximately 1595 cm⁻¹. This result demonstrates that GO samples are distorted in the sp² crystal structure and exhibit defects (Aliyev et al., 2019). The intensity ratio (I_D/I_G) of GO samples, 0.85, indicates the presence of sp² carbon networks and an increase in edge planes and various disorders, including defects, ripples, and wrinkles found in SEM analysis (Krishnamoorthy et al., 2013). Other studies reported an intensity ratio of 0.83 to 0.93 due to oxygen functionalities present at defect sites (Xing et al., 2020; Zhang et al., 2018b). Weak and broad 2D peaks at around 2690 cm⁻¹ also indicate a disorder that can be attributed to double resonance transitions, resulting in the production of two phonons with opposite momentum (Krishnamoorthy et al., defect-activated peak called D+G is visible near 2960 cm⁻¹.

XRD analysis was employed to assess the structure of the synthesized GO (Krishnamoorthy et al., 2013). For graphite, one sharp peak can be observed at a 20 of 26.61° (Figure SI-1). This peak confirms the presence of a well-ordered layered structure with 0.334 nm d-spacing along the (002) orientation and is in agreement with the reference XRD pattern (ICDD File 9,012,230) (Zhang et al., 2019; Hidayah et al., 2017). Upon oxidation of graphite, its crystal structure is altered: the 20 peak at 11.4° for GO indicates that the graphite was fully oxidized. Furthermore, the interlayer distance of GO reveals a d-spacing of 0.775 nm. The increase in interlayer spacing of GO from graphite is attributed to the intercalation of oxygenated functional groups. The XRD findings of the GO are consistent with other studies (Guerrero et al., 2015; Krishnamoorthy et al., 2013). Characterization with SEM, EDX mapping, FTIR, Raman,

and XRD patterns demonstrate properties consistent with GO.

Characterization results provide insight into how GO will interact with the microbial population present in the BAF system. For example, in this study, SEM results showed wrinkled, corrugated, and folded structures of GO surface with various defects and ripples, as confirmed by Raman analysis. Such morphology increases surface roughness and leads to strong adhesion of microbes, inducing growth (Zhang and Tremblay, 2020). Moreover, FTIR and EDX results suggested that the GO sheets used in this study include hydrophilic oxygenated groups on their surfaces, enabling them to produce a stable dispersion in water. XRD result suggests that GO was fully exfoliated in water and increased its specific surface area (Zhang et al., 2020). The greater surface area of GO provides a suitable environment for bacterial cell adhesion by offering more reaction sites (Braylé et al., 2022; Sanchez et al., 2012). The basal plane of GO enables biological cell attachment by noncovalent interactions, whereas edges help adhere to biological molecules through covalent interactions (Hui et al., 2014). Additionally, impurities were not observed on the GO surface. With increased interactions with microbial populations in the BAF system, GO stimulated biodegradation rates, that is expected to have a beneficial impact on CECs treatment compared to conventional GAC and GAC-BAFs, decreasing treatment time and cost.

3.2. Role of GO on ROS generation and oxidative stress

ROS generation, one of the primary factors for cellular dysfunction, is often proposed as a common toxicological mechanism for GO. Studies have indicated that GO may induce oxidative stress by directly generating ROS (Guo et al., 2017; Pelin et al., 2018; Song et al., 2018). To further investigate the toxicity of GO to GAC-BAF, ROS production during biofilm formation was measured using an NBT assay. The results showed that during the exponential growth phase (up to 30 h), compared to the control, the presence of GO showed no effect on ROS generation under all concentrations examined (Fig. 2). Interestingly, continued exposure to 48 h revealed a decrease in ROS generation by as much as 30 % (p > 0.05) compared to the control batch. These results suggest that oxidative stress observed due to exposure to GO was less than the control (w/o GO), decreased with time, and did not affect cell proliferation during the exponential phase. Prior studies also reported such time-dependent ROS generation while exposed to GO concentrations (Evariste et al., 2021; Guo et al., 2017; Siqueira et al., 2022). For example, Siqueira et al. (2022) reported that zebrafish liver cells exposed to GO produced less ROS after 72 h than 24 h compared to control. This time-dependent ROS generation of GO can be ascribed to the cells' physiological state, which differs at each maturation stage (Fallatah et al., 2019). In another study, Guo et al. (2017) investigated the effects of GO on biofilm formation in pure bacterial cultures and reported that GO enhanced microbial growth and biofilm formation up to 500 mg/L without producing significant ROS at the GO concentration range of 5-100 mg/L. In this experiment, H₂O₂ was used as a positive control as it stimulates ROS production. The presence of 3 mM H₂O₂ resulted in a significant increase (60%) in ROS levels compared to the ROS intensity observed in the control (Fig. 2).

3.3. Effects of GO on microbial growth and biofilm formation

The microbial interaction of GO was assessed through ATP analysis by exposing the microbial community of GAC-BAF to GO concentrations from 25 μ g/L to 1000 μ g/L over 48 h. Based on ATP concentrations observed, GO was biocompatible with the GAC-BAF, showing no toxicity effect on viable cells within the biofilm (Fig. 3a). The initial ATP concentration in the GAC-BAF was 26–70 ng ATP/cm³ GAC. Zhang et al. (2017) reported the initial ATP concentration of a 2-year BAF as 5–62 ng ATP/cm³ GAC from PVWC, and after reaching steady-state conditions in the lab, ATP concentrations increased up to 350 ng ATP/cm³ GAC. On the other hand, Velten et al. (2011) reported an initial ATP

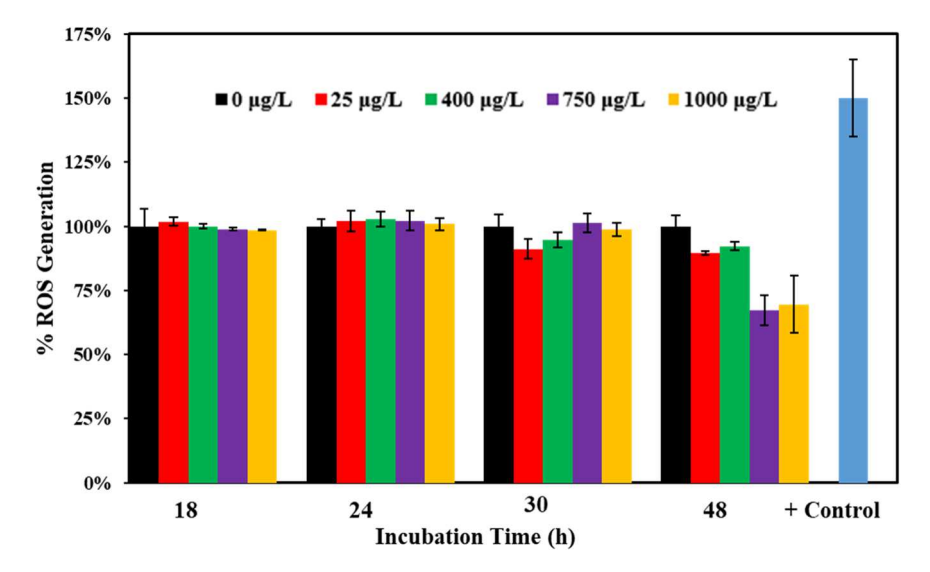


Fig. 2. ROS generation in GAC-BAF biofilm after incubation with varying GO concentrations. + Control indicates H₂O₂ as an oxidizing agent.

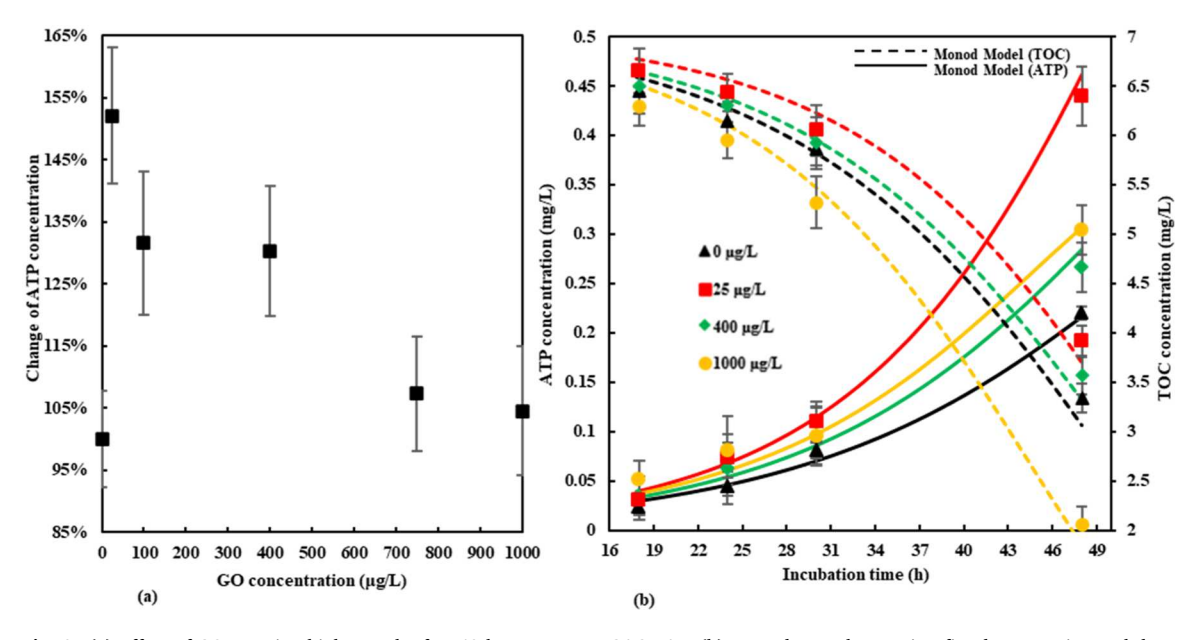


Fig. 3. (a) Effect of GO on microbial growth after 48 h exposure to GAC-BAF; (b) Monod growth equation fitted to experimental data.

concentration of 9.32 ng ATP/cm³ GAC and a steady-state concentration of 500 ng ATP/cm³ GAC for a drinking water GAC filter. In our study, the average ATP concentration of GAC-BAF increased up to 660 ng ATP/cm³ GAC after 48 h without GO (control). However, ATP concentrations increased in the presence of GO at 25 μ g/L (52 %) and 400 μ g/L (30 %) (Fig. 3a). Although ATP concentrations increased as well at higher GO concentrations (750–1000 $\mu g/L$), they peaked in the range of 25 to 40 μ g/L. The GO used in this study formed a stable dispersion because of the oxygenated groups on its surfaces, increasing the potential to interact with microbial cells and thus induce cell differentiation and proliferation (Chen et al., 2014). These results are consistent with several studies with pure bacterial cultures where significant bacterial growth was observed in the presence of GO (Chen et al., 2014; Guo et al., 2017; Ruiz et al., 2011; Song et al., 2018). For example, Wang et al. (2013) reported that the microbial activity of anammox bacteria was enhanced (10.26 %) with GO at 100 mg/L. Another study by Yin et al. (2015) reported that GO doses ranging from 0 to 100 mg/L increased anammox bacteria activity, which enhanced nitrogen removal by 17.2 % compared to that of the control experiment. Furthermore, GO enhanced extracellular polymeric substances (EPS), increasing energy for the catabolism of anammox cells (Wang et al., 2013). Moreover, EPS supports microcolonies that potentially increase the activity of bacteria (Yin et al., 2015). GO sheets can form membrane scaffolds for bacterial attachment and proliferation and also improve the mass transfer of nutrients and metabolites between the bulk medium and bacteria, inducing growth (Chen et al., 2014; Wang et al., 2013). Song et al. (2018) found that the presence of GO, even up to 10 mg/L, enhanced the biofilm formation of E. coli in a pure culture medium by 50 %. To explain the biofilm formation mechanism, authors proposed that lower GO doses may inactivate some microbial cells, resulting in a protective barrier to prevent the other cells from contact with GO, and dead cells act as nutrient sources for the remaining living cells, thus increasing biofilm formation (Song et al., 2018). In our study, although the concentration of GO was comparatively low, consistent with biomass concentrations in water treatment plants, the loading of GO to biomass based on ATP was

The growth rate and substrate consumption (TOC) were modeled with the Monod Equations (Eqs. (1) and 2) to obtain best-fit rate

constants (Liu, 2017). The mass balance for ATP and TOC, respectively, in the batch reactor follows:

$$\frac{dX}{dt} = \frac{\mu_{max} S}{K_s + S} \times X \tag{1}$$

$$\frac{dS}{dt} = -\frac{\mu_{max}}{K_s + S} \times \frac{X}{Y}$$
 (2)

Where μ_{max} is the maximum specific growth rate (h⁻¹), X is the ATP concentration (mg/L), K_S is the Monod half-saturation constant (mg/L), S is the substrate TOC concentration (mg/L), t is the incubation time (h), and Y is the biomass yield factor. An apparent lag time of 6 h was observed, and after that, the cell concentration transitioned to an exponential pattern (Figure SI-2). Solving the equations simultaneously, kinetic parameters were acquired (Table SI-2). After 48 h of incubation, the maximum growth rate μ_{max} in the control batch was $0.111 \pm 0.025 \ h^{\text{--}1}$ (Table SI-2). The growth rates of microbes increased when exposed to GO concentrations, with the greatest maximum growth rate of $0.162 \pm 0.026 \text{ h}^{-1}$ at 25 µg/L (Fig. 3b). Moreover, GO-exposed BAF samples showed slightly higher K_S values of 4.06-5.05 mg/L compared to the control sample (3.52 mg/L), suggesting less affinity of cells to the substrate (Table SI-2). Enhanced biofilms with high cell density due to the interaction of GO would lead to such a larger value of the K_S (Liu, 2007).

As discussed earlier, source water was prepared to simulate the influent water composition of the treatment plant and nutrient concentrations were adapted from a previous study (Zhang et al., 2017). Briefly, carbon, nitrogen, and phosphorus were added at a mass ratio of 15:5:1 ensuring microbial growth as applied in earlier studies focused on

drinking water biofilters (Liu et al., 2001; Urfer and Huck, 2001). Moreover, this study was conducted for a short duration (48 h) to evaluate the microbial growth parameters (i.e., μ_{max} , K_S , and Y) during the exponential growth phase. These parameters will be used to design column reactors for a full-scale BAF system, reducing the time, effort, and cost associated with pilot studies (Acevedo et al., 2021; Badriyha et al., 2003; Yuan et al., 2022). BAFs and other biological processes must run at steady-state conditions in water treatment.

3.4. Interaction of GO with GAC-BAF samples

SEM images demonstrate the morphology and structure of biofilm upon exposure to GO concentrations and provide visible evidence of how GO sheets interact with bacterial cells. The SEM images (Fig. 4) show that after exposure to GO for 48 h, the cell membranes remained integrated, similar to the untreated BAF samples, and there were no noticeable changes in cell structure. No evidence of wrapping was found for GO in this study. Instead, GO sheets at higher concentrations (1000 μg/L) were observed to create a thin membrane that covered the surface of bacterial cells (Fig. 4(c-d)). These results suggest that such thin membranes may act as a scaffold for bacterial attachment, proliferation, and biofilm formation (Chen et al., 2014). Our results are consistent with several prior studies suggesting that GO showed no toxicity and could serve as a nonspecific promoter of cellular growth (Guo et al., 2017; Ruiz et al., 2011). Because of its hydrophilic nature, GO used in this study can produce a stable suspension in the growth media at lower concentrations (25 µg/L), thereby serving as a platform for increased bacterial adhesion and proliferation even though no visible GO sheets were observed (Fig. 4b). Other studies reported that GO could act as a

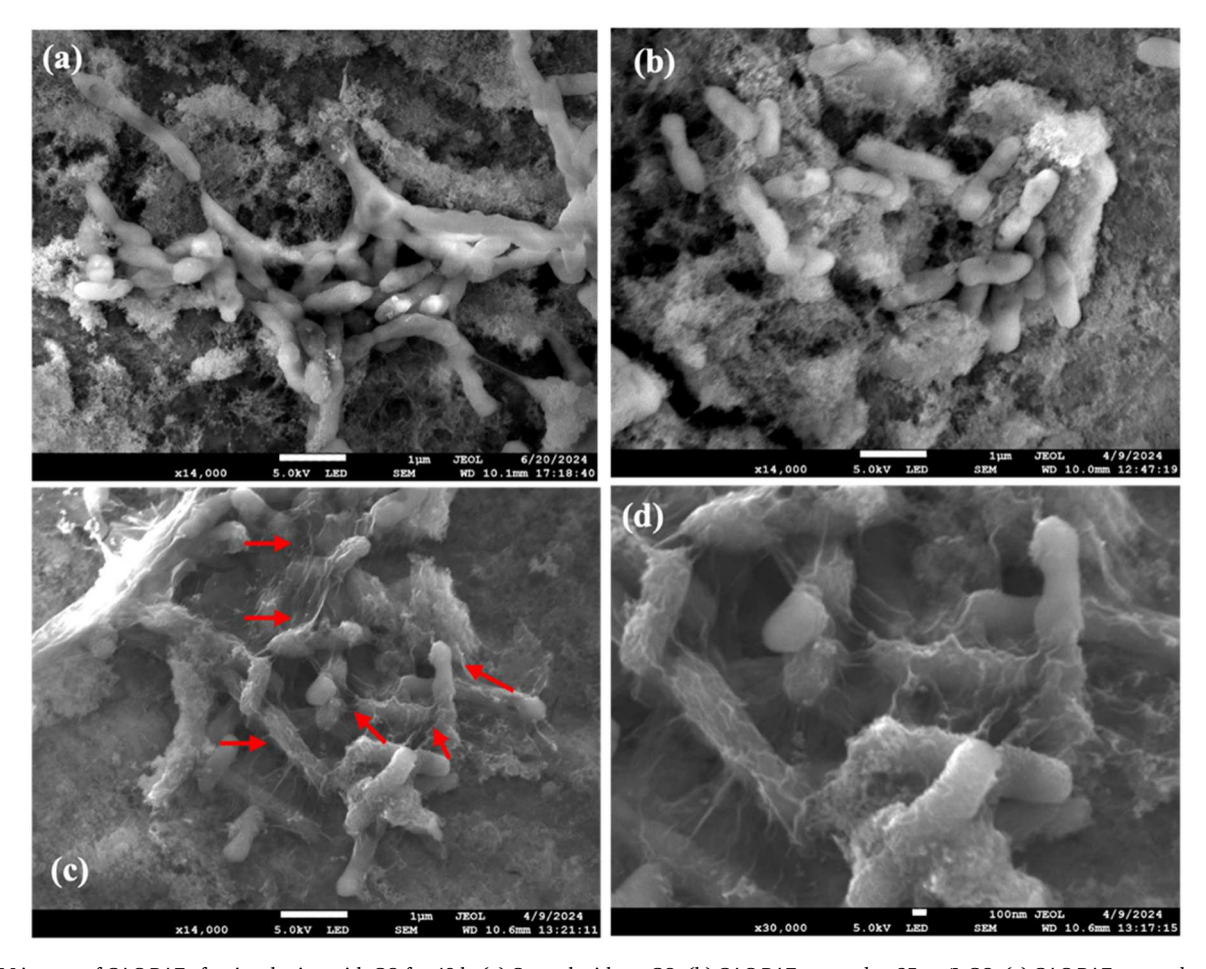


Fig. 4. SEM images of GAC-BAF after incubation with GO for 48 h. (a) Control without GO; (b) GAC-BAF exposed to $25 \,\mu\text{g/L}$ GO; (c) GAC-BAF exposed to $1000 \,\mu\text{g/L}$ GO; (d) Higher magnifications of the regions in (c) as shown by the red arrows. Red arrows indicate the presence of GO sheets on the GAC-BAF sample.

platform for concentrating nutrients to facilitate microbial growth (Chen et al., 2014; Guo et al., 2017).

3.5. Richness and diversity of bacterial communities upon exposure to GO

To further explore the structure and biodiversity of the BAF microbial community upon exposure to GO concentrations, samples were collected after 48 h, and the 16S rRNA gene was amplified and sequenced using high throughput sequencing. Two 16S rRNA libraries were constructed via high-throughput sequencing of the bacterial

communities from the GO-exposed BAF samples (BAF w/GO $_{25}$ and BAF w/GO $_{1000}$) and the control without GO sample (BAF w/o GO) generating 730,454, 467,385 and 435,908 high-quality reads respectively (**Table SI-3**). The mean quality score ($Q=-10\log_{10}$ (p) where p represents the probability that the base calling is incorrect) for the DNA sequencing was 35.54, with an average % base of 91.58. For base calls with a quality score of 35.54, approximately 3 base calls in 10,000 were predicted to be incorrect; therefore, most of the reads were reliable data without errors (Kwon et al., 2013). There were 1427, 1504, and 1484 operational taxonomic units (OTUs) found in BAF (w/o GO), BAF

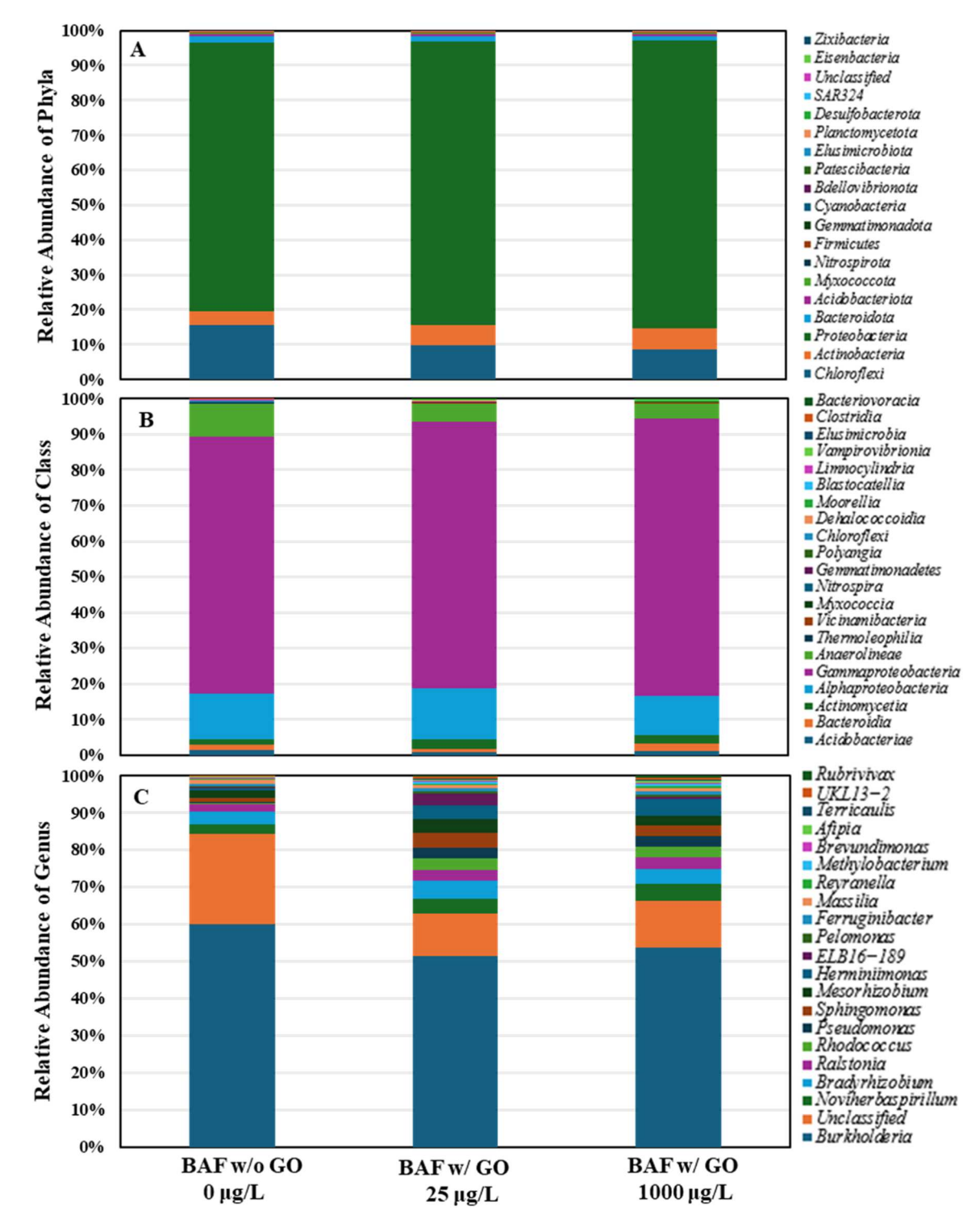


Fig. 5. Relative abundance of microbial communities in BAF samples after exposure to GO concentrations: (A) Phylum level, (B) Class level, and (C) Genus level.

(w/GO₂₅), and BAF (w/GO₁₀₀₀), respectively, with a minimal relative abundance at 3 %. The Chao1 and abundance coverage estimator (ACE) indices for richness and the Simpson and Shannon indices for diversity in the BAF samples exposed to different GO concentrations were assessed (Table SI-3). Greater Chao1 and ACE indexes with GO exposure indicate that GO promotes the growth of some bacteria and increases their richness to a certain extent. GO exposure increased the Chao1 and ACE indices compared to the control, peaking at 25 µg/L followed by a decrease at 1000 μ g/L. The overall trend of Chao1 revealed BAF w/GO₂₅ > BAF w/GO $_{1000}$ > BAF w/o GO; ACE, BAF w/GO $_{25}$ > BAF w/GO $_{1000}$ >BAF w/o GO. Based on the Simpson and Shannon indices, greater diversity was observed in GO-exposed BAF samples (3.43-3.52) compared to the BAF without GO (3.0). Moreover, lower GO concentrations increased the richness of the microbial communities, whereas higher GO concentrations increased the microbial diversity of the BAF samples compared to the BAF without GO. Consistent with other studies (Du et al., 2015; Lian et al., 2020; Yan et al., 2021), these results revealed that BAF samples without GO exhibited less diversity than BAF samples exposed to GO, suggesting a more diverse bacterial community formed and attached to the BAF sample while interacting with GO.

3.6. Composition distinction between GO-exposed BAF samples at different taxonomic levels

To characterize the changes in the BAF microbial community upon exposure to GO concentrations, the bacterial OTUs were assigned to phyla (Fig. 5A), classes (Fig. 5B), and genera (Fig. 5C). Eighteen bacterial phyla were identified in both BAF and GO-exposed BAF samples, with Proteobacteria emerging as the predominant one. The detection of Proteobacteria as the most dominant phyla was expected. Prior studies also reported similar observations in water treatment plants where Proteobacteria were the most abundant in filter media (Liao et al., 2013; Zhang et al., 2018). In the BAF without GO, the relative abundance of Proteobacteria was 77.1 %, followed by Chloroflexi (15.69 %), Actinobacteria (4%), and Bacteroidota (1%) (Fig. 5A). In an earlier study, Dong et al. (2018) also reported the relative abundance of Proteobacteria as 87 %, followed by Firmicutes (8 %), Bacteroidetes (4 %), and Actinobacteria (1 %) on GAC biofilm collected from a fluidized bed reactor. However, results showed that the relative abundance of major microbial communities in BAF samples varied with the applied GO concentrations. GO exposure increased the relative abundance of Proteobacteria (81 % to 83 %) and Actinobacteria (6 % to 7 %) but decreased that of Chloroflexi (10 % to 8 %). Similar trends were also observed at the class level (Fig. 5B); all samples showed a high proportion of *Gammaproteobacteria* (72 %–78 %), α -Proteobacteria (11 %-14.50 %), Anaerolineae (4 %-9.5 %), and Actinomycetia (1.4 %-2.5 %), which accounted for >98 % of the total abundance of the bacterial classes (Fig. 5B). Differences in bacterial classes in all BAF and GO-exposed BAF samples were detected and consistent with the results observed in bacterial phyla. These results are consistent with several studies where Du et al. (2015) reported Proteobacteria (24.23 %) and Chloroflexi (18.17 %) as the dominant phyla in the bacterial community of GO-exposed soil samples and Yan et al. (2021) observed Proteobacteria (60.46 %) and Firmicutes (19.59 %) in GO-treated wastewater samples. Microbial communities in both BAF and GO-exposed BAF samples showed no significant difference at the phylum and class levels, which is consistent with other studies (Du et al., 2015; Lian et al., 2020). However, greater differences were observed at the genus level for Noviherbaspirillum, Bradyrhizobium, Ralstonia, Mesorhizobium, and Herminiimonas (Fig. 5C).

Community composition at the genus level with a minimal relative abundance of 3 % accounted for 76 % of the BAF community without GO, 80% w/GO₂₅, and 81% w/GO₁₀₀₀ among the total genus-related assigned sequences (Fig. 5C). Greater variations in the top 20 abundant genera were observed, 75 % of which belonged to phyla *Proteobacteria* for the BAF community without GO, 71% w/GO₂₅, 72% w/GO₁₀₀₀. Among all the genera, *Burkholderia* is the most dominant, which

belongs to the Proteobacteria phyla. Other studies also reported the presence of the Burkholderia genus in water treatment, which can tolerate and degrade various aromatic compounds (Cauduro et al., 2021; Morya et al., 2020). Differences at the other genus level were observed as well when BAF samples were exposed to GO concentrations. For BAF w/o GO, 2.7 % of Noviherbaspirillum, 3.3 % of Bradyrhizobium, 2 % of Ralstonia, 2 % of Mesorhizobium, 0.9 % of Sphingomonas, and 0.75 % of Herminiimonas were observed; however, after exposure to GO concentrations changes resulted in overall increases in abundances (Fig. 5C). All of these enriched genera belong to the Proteobacteria phylum and are known as potential CEC degraders reported in other studies (Wang et al., 2018; Yan et al., 2021; Zhang et al., 2018). It appears that several sequences (25 % for BAF w/o GO, 20 % BAF w/GO25, and 21 % BAF w/GO₁₀₀₀) are assigned as unclassified, most of which belong to Chloroflexi phyla. Prior studies reported that the microbial community developed in GAC-BAF samples not only depends on the community in the source water but is also affected by the water chemistry (e.g., nutrient concentration, background electrolyte, contaminants and CECs) (Zhang et al., 2018; Zhou and Xu, 2020). In this study, GO was spiked into the system, and results showed that the bacterial population developed in the BAF sample is affected by the presence of GO in the source water, specifically at the genus level, which is consistent with other studies (Du et al., 2015; Kedves et al., 2020; Yan et al., 2021).

3.7. Implication to the water treatment system

Prior studies demonstrated that GAC-supported BAFs were effective as an advanced water treatment process for CECs, including pesticides, analgesics, and antibiotics at environmentally relevant concentrations (Zhang et al., 2016, 2017). However, due to its microporosity, organic contaminants partition and diffuse into GAC. As a result, microorganisms may not have ready access to degrade organic compounds, potentially extending treatment time and costs (Lu et al., 2020). In a mixed-media process of GO-GAC-BAF, the benefits of GO include increasing microbial growth as well as serving as a surface for increased surface interactions with CECs. Mixed-media biofilters have recently been gaining attention in treating CECs (Li et al., 2022) where, for example, Li et al. (2018) successfully treated pharmaceuticals and personal care products (PPCPs) with a bench-scale GAC sandwiched slow sand filter (SSFs) as did Xu et al. (2021). Recent works with GO-GAC composites have shown greater adsorption capacity than GAC and sand (Ahamed et al., 2020; Bhattacharyya et al., 2021; Januário et al., 2022; Ndagijimana et al., 2023). A GAC-based mixed media BAF, optimized with a GO-GAC composite, is expected to increase adsorption capacity, further contributing to biodegradation rates by enhancing microbial growth compared to sand and GAC. As such, parameters (i.e., μ_{max} , K_{S} , and Y) determined in this study are important for modeling a full-scale BAF system (Acevedo et al., 2021; Terry et al., 2019; Yuan et al., 2022). Moreover, the input parameters determined from this bench-scale study would reduce the need for expensive and time-consuming pilot-scale investigations.

4. Conclusion

The primary focus of this study was to assess interactions between GO and the microbial community of biologically active filters from a water treatment plant. Results demonstrated that GO did not increase ROS levels during the exponential growth phase compared to the control samples without GO. Interestingly, the presence of GO resulted in significant increases in ATP concentrations, up to 52 %, compared to the control batch. The Monod equation also revealed that GO suspension increased growth rates over the duration of the study by 20 %- 46 % compared to the control batch. Moreover, our observations indicate that GO sheets can form an effective scaffold to promote microbial adhesion and proliferation. These results suggest that GO is biocompatible and could be impregnated into GAC to develop a bio-optimized GAC-BAF

system as an advanced and sustainable water treatment process for treating CECs. Moreover, results demonstrated that the composition and dynamics of BAF microbial communities changed when exposed to GO, as revealed by high-throughput sequencing. Overall, this is the first study to demonstrate the effect of GO on the properties and growth of a GAC-based BAF used in water treatment. This research provides a foundation for the future advancement of bio-optimized BAF systems for water treatment and reuse.

CRediT authorship contribution statement

Tanvir Ahamed: Writing – original draft, Visualization, Software, Methodology, Investigation, Formal analysis, Conceptualization. **Chao Li:** Methodology, Formal analysis. **Mengyan Li:** Writing – review & editing, Resources, Project administration. **Lisa Axe:** Writing – review & editing, Validation, Supervision, Resources, Project administration, Methodology, Conceptualization.

Declaration of competing interest

The authors declare that they have no known competing financial interests or personal relationships that could have appeared to influence the work reported in this paper.

Data availability

Data will be made available on request.

Acknowledgment

We acknowledge the National Science Foundation (Grant Number CBET -1903597) and the New Jersey Water Resources Research Institute (NJWRRI) FY2023 for financial support. The authors thank Wendy Simone and Dave Melnick from the Passaic Valley Water Commission in Totowa, NJ, for their support in collecting and using samples from their GAC filter. The authors would also like to thank the Materials Characterization Center at the New Jersey Institute of Technology for help with instrument training. Additional thanks to Samina Sarwar in the Chemical Engineering Department for help with the SEM. Special thanks to Jose Antunes from the Chemistry and Environmental Science Department for helping with DNA extraction and PCR amplification.

Supplementary materials

Supplementary material associated with this article can be found, in the online version, at doi:10.1016/j.watres.2024.122155.

References

- Acevedo Alonso, V., Kaiser, T., Babist, R., 2021. A multi-component model for granular activated carbon filters combining biofilm and adsorption kinetics. Water Res. 197, 117079 https://doi.org/10.1016/j.watres.2021.117079.
- Ahamed, T., Brown, S.P., Salehi, M., 2020. Investigate the role of biofilm and water chemistry on lead deposition onto and release from polyethylene: an implication for potable water pipes. J. Hazard. Mater. 400 (March), 123253 https://doi.org/ 10.1016/i.ihazmat.2020.123253.
- Alam, S.N., Sharma, N., Kumar, L., 2017. Synthesis of graphene oxide (GO) by modified hummers method and its thermal reduction to obtain reduced graphene Oxide (rGO) *. Graphene 06 (01), 1–18. https://doi.org/10.4236/graphene.2017.61001.
- Aliyev, E., Filiz, V., Khan, M.M., 2019. Structural characterization of graphene oxide: surface functional groups and fractionated oxidative debris. Nanomaterials 9 (8), 1180. https://doi.org/10.3390/nano9081180.
- Anand, A., Unnikrishnan, B., Huang, C.C., 2019. Graphene oxide and carbon dots as broad-spectrum antimicrobial agents-a minireview. Nanoscale Horiz. 4 (1), 117–137. https://doi.org/10.1039/c8nh00174i.
- Andrade, M.B., Santos, T.R.T., Fernandes Silva, M., Vieira, M.F., Bergamasco, R., Hamoudi, S., 2019. Graphene oxide impregnated with iron oxide nanoparticles for the removal of atrazine from the aqueous medium. Sep. Sci. Technol. 54 (16), 2653–2670. https://doi.org/10.1080/01496395.2018.1549077.

Andrijanto, E., Subiyanto, G., Lintang, C., 2018. Preparation of graphene oxide sand composites as super adsorbent for water purification application. MATEC Web Conf. 156, 1–5. https://doi.org/10.1051/matecconf/201815605019.

- Azizi-Lalabadi, M., Hashemi, H., Jafari, S.M., 2020. Carbon nanomaterials against pathogens; the antimicrobial activity of carbon nanotubes, graphene/graphene oxide, fullerenes, and their nanocomposites. Adv. Colloid Interface Sci. 284, 102250 https://doi.org/10.1016/j.cis.2020.102250.
- Badriyha, B.N., Ravindran, V., Den, W., 2003. Bioadsorber efficiency, design, and performance forecasting for alachlor removal. Water Res. 37 (17), 4051–4072. https://doi.org/10.1016/S0043-1354(03)00266-5.
- Bhattacharyya, A., Ghorai, S., Rana, D., Roy, I., Sarkar, G., Saha, N.R., Orasugh, J.T., De, S., Sadhukhan, S., Chattopadhyay, D., 2021. Design of an efficient and selective adsorbent of cationic dye through activated carbon graphene oxide nanocomposite: study on mechanism and synergy. Mater. Chem. Phys. 260 (November 2020), 124090 https://doi.org/10.1016/j.matchemphys.2020.124090.
- Boulanger, N., Kuzenkova, A.S., Iakunkov, A., Nordenström, A., Romanchuk, A.Y., Trigub, A.L., Zasimov, P.V., Prodana, M., Enachescu, M., Bauters, S., Amidani, L., Kvashnina, K.O., Kalmykov, S.N., Talyzin, A.V., 2022. High surface area "3D Graphene Oxide" for enhanced sorption of radionuclides. Adv. Mater. Interfaces 9 (18). https://doi.org/10.1002/admi.202200510.
- Braylé, P., Pinelli, E., Gauthier, L., Mouchet, F., Barret, M., 2022. Graphene-based nanomaterials and microbial communities: a review of their interactions, from ecotoxicology to bioprocess engineering perspectives. Environ. Sci.: Nano 9 (10), 3725–3741. https://doi.org/10.1039/D2EN00547F.
- Cauduro, G.P., Leal, A.L., Mahenthiralingam, E., Valiati, V.H., 2021. New benzo(a) pyrene-degrading strains of the Burkholderia cepacia complex prospected from activated sludge in a petrochemical wastewater treatment plant. Environ. Monit. Assess 193 (4), 163. https://doi.org/10.1007/s10661-021-08952-z.
- Chen, H.Q., Gao, D., Feng, W.Y., 2014. Graphene oxide as an anaerobic membrane scaffold for the enhancement of B. adolescentis proliferation and antagonistic effects against pathogens E. coli and S. aureus. Nanotechnology 25 (16). https://doi.org/10.1088/0957-4484/25/16/165101.
- Coyle, C.H., Martinez, L.J., Coleman, M.C., Spitz, D.R., Weintraub, N.L., Kader, K.N., 2006. Mechanisms of H202-induced oxidative stress in endothelial cells. Free Radical Biol. Med. 40 (12), 2206–2213. https://doi.org/10.1016/j.freeradbiomed.2006.02.017.
- Dasari, B.L., Nouri, J.M., Naher, S., 2017. Graphene and derivatives synthesis techniques, properties and their energy applications. Energy 140, 766–778. https://doi.org/10.1016/j.energy.2017.08.048.
- Dong, Z., Wang, H., Tian, S., Xie, J., 2018. Fluidized granular activated carbon electrode for efficient microbial electrosynthesis of acetate from carbon dioxide. Bioresour. Technol. 269, 203–209. https://doi.org/10.1016/j.biortech.2018.08.103.
- Du, J., Hu, X., Zhou, Q., 2015. Graphene oxide regulates the bacterial community and exhibits property changes in soil. RSC Adv. 5 (34), 27009–27017. https://doi.org/ 10.1039/c5ra01045d.
- Edgar, R.C., 2010. Search and clustering orders of magnitude faster than BLAST. Bioinformatics. 26 (19), 2460–2461. https://doi.org/10.1093/bioinformatics/btq461.
- Engelbrecht, I., Horn, S., Giesy, J.P., Pieters, R., 2024. A method to determine reactive oxygen species production in intestinal and liver cell cultures using the 2',7'dichlorodihydrofluorescein diacetate assay. MethodsX 12 (September 2023), 102615. https://doi.org/10.1016/j.mex.2024.102615.
- Evariste, L., Braylé, P., Barret, M., 2021. Graphene-based nanomaterials modulate internal biofilm interactions and microbial diversity. Front. Microbiol. 12 https://doi.org/10.3389/fmicb.2021.623853
- Fallatah, H., Elhaneid, M., Gkatzionis, K., 2019. Antibacterial effect of graphene oxide (GO) nano-particles against Pseudomonas putida biofilm of variable age. Environ. Sci. Pollut. Res. 26 (24), 25057–25070. https://doi.org/10.1007/s11356-019-05688-9.
- Forstner, C., Orton, T.G., Skarshewski, A., Wang, P., Kopittke, P.M., Dennis, P.G., 2019. Effects of graphene oxide and graphite on soil bacterial and fungal diversity. Sci. Total Environ. 671, 140–148. https://doi.org/10.1016/j.scitotenv.2019.03.360.
- Gao, Y., Li, Y., Shah, S.M., Su, X., 2012. Adsorption and removal of tetracycline antibiotics from aqueous solution by graphene oxide. J. Colloid Interface Sci. 368 (1), 540–546. https://doi.org/10.1016/j.jcis.2011.11.015.
- Grande, C.D., Mangadlao, J., Fan, J., Rodrigues, D.F., Advincula, R., 2017. Chitosan cross-linked graphene oxide nanocomposite films with antimicrobial activity for application in food industry. Macromol. Symp. 374 (1), 1–8. https://doi.org/ 10.1002/masy.201600114.
- Guerrero-Contreras, J., Caballero-Briones, F., 2015. Graphene oxide powders with different oxidation degree, prepared by synthesis variations of the hummers method. Mater. Chem. Phys. 153, 209–220. https://doi.org/10.1016/j.
- Guo, Z., Xie, C., Zhang, P., Zhang, Z., 2017. Toxicity and transformation of graphene oxide and reduced graphene oxide in bacteria biofilm. Sci. Total Environ. 580, 1300–1308. https://doi.org/10.1016/j.scitotenv.2016.12.093.
- Gurunathan, S., Han, J.W., Eppakayala, V., Kim, J.H., 2012. Oxidative stress-mediated antibacterial activity of graphene oxide and reduced graphene oxide in Pseudomonas aeruginosa. Int. J. Nanomed. 7, 5901–5914. https://doi.org/10.2147/ LJN.S37397.
- Hess, A., Morgenroth, E., 2021. Biological activated carbon filter for greywater post-treatment: long-term TOC removal with adsorption and biodegradation. Water. Res. X. 13, 100113 https://doi.org/10.1016/j.wroa.2021.100113.
- Hidayah, N.M.S., Liu, W.-W., Lai, C.-W., 2017. Comparison on graphite, graphene oxide and reduced graphene oxide: synthesis and characterization. In: AIP Conference Proceedings, 1892, 150002. https://doi.org/10.1063/1.5005764.

- Hui, L., Piao, J.-G., Auletta, J., 2014. Availability of the basal planes of graphene oxide determines whether it is antibacterial. ACS Appl .Mater. Interfaces 6 (15), 13183–13190. https://doi.org/10.1021/am503070z.
- Hulagabali, M.M., Vesmawala, G.R., Patil, Y.D., 2023. Synthesis, characterization, and application of graphene oxide and reduced graphene oxide and its influence on rheology, microstructure, and mechanical strength of cement paste. J. Build. Eng. 71, 106586 https://doi.org/10.1016/j.jobe.2023.106586.
- Hummers, W.S., Offeman, R.E., 1958. Preparation of graphitic oxide. J. Am. Chem. Soc. 80 (6), 1339. https://doi.org/10.1021/ja01539a017. -1339.
- Januário, E.F.D., Fachina, Y.J., Wernke, G., Demiti, G.M.M., Beltran, L.B., Bergamasco, R., Vieira, A.M.S., 2022. Application of activated carbon functionalized with graphene oxide for efficient removal of COVID-19 treatment-related pharmaceuticals from water. Chemosphere 289 (December 2021), 133213. https:// doi.org/10.1016/j.chemosphere.2021.133213.
- Jørgensen, P.E., Eriksen, T., Jensen, B.K., 1992. Estimation of viable biomass in wastewater and activated sludge by determination of ATP, oxygen utilization rate and FDA hydrolysis. Water Res. 26 (11), 1495–1501. https://doi.org/10.1016/0043-1354(92)00069-G.
- Kedves, A., Sánta, L., Balázs, M., Kónya, Z., 2020. Chronic responses of aerobic granules to the presence of graphene oxide in sequencing batch reactors. J. Hazard. Mater. 389, 121905 https://doi.org/10.1016/j.jhazmat.2019.121905.
- Krishnamoorthy, K., Veerapandian, M., Yun, K., Kim, S.J., 2013. The chemical and structural analysis of graphene oxide with different degrees of oxidation. Carbon N Y 53, 38–49. https://doi.org/10.1016/j.carbon.2012.10.013.
- Kumar, P., Pérez, J.A.E., Knystautas, É., 2020. Removal of microcystin-LR and other water pollutants using sand coated with bio-optimized carbon submicron particles: graphene oxide and reduced graphene oxide. Chem. Eng. J. 397, 125398 https://doi. org/10.1016/j.cej.2020.125398.
- Li, C., Zeng, W., Li, N., Guo, Y., Peng, Y., 2019a. Population structure and morphotype analysis of "candidatus accumulibacter" using fluorescence in situ hybridizationstaining-flow cytometry. Appl. Environ. Microbiol. 85 (9) https://doi.org/10.1128/ AEM.02943-18.
- Li, J., Campos, L.C., Zhang, L., Xie, W., 2022. Sand and sand-GAC filtration technologies in removing PPCPs: a review. Sci. Total Environ. 848, 157680 https://doi.org/ 10.1016/j.scitotenv.2022.157680.
- Li, J., Zhou, Q., Campos, L.C., 2018. The application of GAC sandwich slow sand filtration to remove pharmaceutical and personal care products. Sci. Total Environ. 635, 1182–1190. https://doi.org/10.1016/j.scitotenv.2018.04.198.
- Li, N., Zeng, W., Guo, Y., Li, C., Ma, C., Peng, Y., 2019b. Nitrogen-associated niche characteristics and bacterial community estimated by 15N-DNA-stable isotope probing in one-stage partial nitritation/anammox process with different ammonium loading. J. Environ. Manage. 247 (100), 603–612. https://doi.org/10.1016/j. ienyman.2019.06.110.
- Lian, S., Qu, Y., Deng, Y., 2020. Interaction of graphene-family nanomaterials with microbial communities in sequential batch reactors revealed by high-throughput sequencing. Environ. Res. 184, 109392 https://doi.org/10.1016/j. envres.2020.109392.
- Liao, X., Chen, C., Xie, S., 2013. Changes of biomass and bacterial communities in biological activated carbon filters for drinking water treatment. Process Biochem. 48 (2), 312–316. https://doi.org/10.1016/j.procbio.2012.12.016.
- Litchfield, K., Stanislaw, S., Spain, L., Gallegos, L.L., Rowan, A., Schnidrig, D., Rosenbaum, H., Harle, A., Au, L., Hill, S.M., Tippu, Z., Thomas, J., Thompson, L., Xu, H., Horswell, S., Barhoumi, A., Jones, C., Leith, K.F., Burgess, D.L., Bridger, H., 2020. Representative sequencing: unbiased sampling of solid tumor tissue. Cell Rep. 31 (5), 107550 https://doi.org/10.1016/j.celrep.2020.107550.
- Liu, S., 2017. How Cells Grow. Bioprocess Engineering. Elsevier, pp. 629–697. https://doi.org/10.1016/B978-0-444-63783-3.00011-3.
 Liu, X., Huck, P.M., Slawson, R.M., 2001. Factors affecting drinking water biofiltration.
- Liu, X., Huck, P.M., Slawson, R.M., 2001. Factors affecting drinking water biofiltration. J. /Am. Water Works Assoc. 93 (12), 90–101. https://doi.org/10.1002/j.1551-8833.2001.tb09358.x.
- Liu, Y.-X., Qin, Y., Chen, T., Bai, Y., 2021. A practical guide to amplicon and metagenomic analysis of microbiome data. Protein Cell 12 (5), 315–330. https://doi. org/10.1007/s13238-020-00724-8.
- Liu, Y., 2007. Overview of some theoretical approaches for derivation of the Monod equation. Appl. Microbiol. Biotechnol. 73 (6), 1241–1250. https://doi.org/10.1007/ s00253-006-0717-7.
- Lu, Z., Sun, W., Li, C., 2020. Effect of granular activated carbon pore-size distribution on biological activated carbon filter performance. Water Res. 177, 115768 https://doi. org/10.1016/j.watres.2020.115768.
- Luo, N., Zhang, X.J., 2022. Graphene oxide influences on bacterial community diversity of larix olgensis rhizosphere of haplic cambisols in Northeast China. Eurasian Soil Sci. 55 (10), 1470–1481. https://doi.org/10.1134/S1064229322100106.
- Maeng, S.K., Sharma, S.K., Abel, C.D.T., Magic-Knezev, A., Amy, G.L., 2011. Role of biodegradation in the removal of pharmaceutically active compounds with different bulk organic matter characteristics through managed aquifer recharge: batch and column studies. Water Res. 45 (16), 4722–4736. https://doi.org/10.1016/j. watres.2011.05.043.
- Magic-Knezev, A., van der Kooij, D., 2004. Optimisation and significance of ATP analysis for measuring active biomass in granular activated carbon filters used in water treatment. Water Res. 38 (18), 3971–3979. https://doi.org/10.1016/j. water 2004.06.017
- McDonald, D., Jiang, Y., Karst, S.M., Knight, R., 2023. Greengenes2 unifies microbial data in a single reference tree. Nat. Biotechnol. https://doi.org/10.1038/s41587-023-01845-1

Morya, R., Salvachúa, D., Thakur, I.S., 2020. Burkholderia: an untapped but promising bacterial genus for the conversion of aromatic compounds. Trends Biotechnol. 38 (9), 963–975. https://doi.org/10.1016/j.tibtech.2020.02.008.

- Muniyalakshmi, M., Sethuraman, K., Silambarasan, D., 2020. Synthesis and characterization of graphene oxide nanosheets. Mater. Today: Proc. 21, 408–410. https://doi.org/10.1016/j.matpr.2019.06.375.
- Nahm, F.S., 2016. Nonparametric statistical tests for the continuous data: the basic concept and the practical use. Korean J. Anesthesiol. 69 (1), 8. https://doi.org/ 10.4097/kjae.2016.69.1.8.
- Ndagijimana, P., Rong, H., Ndokoye, P., Mwizerwa, J.P., Nkinahamira, F., Luo, S., Guo, D., Cui, B., 2023. A review on activated carbon/graphene composite-based materials: synthesis and applications. J. Clean. Prod. 417 (March), 138006 https://doi.org/10.1016/j.iclenro.2023.138006
- Neelgund, G.M., Oki, A., Luo, Z., 2013. In situ deposition of hydroxyapatite on graphene nanosheets. Mater. Res. Bull. 48 (2), 175–179. https://doi.org/10.1016/j. materiachyll 2012 08 077.
- Pelin, M., Fusco, L., Tubaro, A., 2018. Graphene and graphene oxide induce ROS production in human HaCaT skin keratinocytes: the role of xanthine oxidase and NADH dehydrogenase. Nanoscale 10 (25), 11820–11830. https://doi.org/10.1039/c8pr0.2933d
- Rognes, T., Flouri, T., Nichols, B., Quince, C., Mahé, F., 2016. VSEARCH: a versatile open source tool for metagenomics. PeerJ 4 (10), e2584. https://doi.org/10.7717/ peeri.2584.
- Ruiz, O.N., Fernando, K.A.S., Wang, B., 2011. Graphene oxide: a nonspecific enhancer of cellular growth. ACS Nano 5 (10), 8100–8107. https://doi.org/10.1021/nn202699t.
- Sanchez, V.C., Jachak, A., Hurt, R.H., 2012. Biological interactions of graphene-family nanomaterials: an interdisciplinary review. Chem. Res. Toxicol. 25 (1), 15–34. https://doi.org/10.1021/tx200339h.
- Sha, Y., Liu, J., Yu, J., Shahbaz, M., 2020. Effect of graphene oxide on the ammonia removal and bacterial community in a simulated wastewater treatment process. J. Environ. Eng. 146 (9), 1–8. https://doi.org/10.1061/(ASCE)EE.1943-7870.0001781.
- Siqueira, P.R., Souza, J.P., Fernandes, M.N., 2022. Concentration- and time-dependence toxicity of graphene oxide (GO) and reduced graphene oxide (rGO) nanosheets upon zebrafish liver cell line. Aquatic Toxicol. 248, 106199 https://doi.org/10.1016/j.aquatox.2022.106199.
- Song, C., Yang, C.-M., Sun, X.-F., 2018. Influences of graphene oxide on biofilm formation of gram-negative and gram-positive bacteria. Environ. Sci. Pollut. Res. 25 (3), 2853–2860. https://doi.org/10.1007/s11356-017-0616-8.
- Kwon, Sunyoung, Park, Seunghyun, Lee, Byunghan, Yoon, Sungroh, 2013. In-depth analysis of interrelation between quality scores and real errors in illumina reads. In: 2013 35th Annual International Conference of the IEEE Engineering in Medicine and Biology Society (EMBC), pp. 635–638. https://doi.org/10.1109/EMBC.2013.6609580.
- Terry, L.G., Pruisner, P., Peterson, E., 2019. Scale-up methodology for biological filtration removal of dissolved organic matter. Environ. Eng. Sci. 36 (4), 405–412. https://doi.org/10.1089/ees.2018.0316.
- Tian, Y., Yu, Z., Wang, D.W., 2021. Graphene oxide: an emerging electromaterial for energy storage and conversion. J. Energy Chem. 55, 323–344. https://doi.org/ 10.1016/j.jechem.2020.07.006.
- Urfer, D., Huck, P.M., 2001. Measurement of biomass activity in drinking water biofilters using a respirometric method. Water Res. 35 (6), 1469–1477. https://doi.org/10.1016/S0043-1354(00)00405-X.
- Vang, Ó.K., Corfitzen, C.B., Smith, C., Albrechtsen, H.-J., 2014. Evaluation of ATP measurements to detect microbial ingress by wastewater and surface water in drinking water. Water Res. 64, 309–320. https://doi.org/10.1016/j. watres.2014.07.015.
- Velten, S., Boller, M., Köster, O., Hammes, F., 2011. Development of biomass in a drinking water granular active carbon (GAC) filter. Water Res. 45 (19), 6347–6354. https://doi.org/10.1016/j.watres.2011.09.017.
- Velten, S., Hammes, F., Boller, M., 2007. Rapid and direct estimation of active biomass on granular activated carbon through adenosine tri-phosphate (ATP) determination. Water Res. 41 (9), 1973–1983. https://doi.org/10.1016/j.watres.2007.01.021.
- Wang, B., Teng, Y., Xu, Y., Chen, W., Luo, Y., 2018. Effect of mixed soil microbiomes on pyrene removal and the response of the soil microorganisms. Sci. Total Environ. 9–17. https://doi.org/10.1016/j.scitotenv.2018.05.290, 640-641.
- Wang, D., Wang, G., Zhang, G., Xu, X., Yang, F., 2013. Using graphene oxide to enhance the activity of anammox bacteria for nitrogen removal. Bioresour. Technol. 131, 527–530. https://doi.org/10.1016/j.biortech.2013.01.099.
- Wang, Y.W., Cao, A., Jiang, Y., Wang, H., 2014. Superior antibacterial activity of zinc oxide/graphene oxide composites originating from high zinc concentration localized around bacteria. ACS Appl. Mater. Interfaces 6 (4), 2791–2798. https://doi.org/ 10.1021/am4053317.
- Wu, X., Tan, S., Xing, Y., Zhao, J.X., 2017. Graphene oxide as an efficient antimicrobial nanomaterial for eradicating multi-drug resistant bacteria in vitro and in vivo. Colloid. Surf. B: Biointerfaces 157, 1–9. https://doi.org/10.1016/j. colsurfb.2017.05.024.
- Xing, R., He, J., Hao, P., Zhou, W., 2020. Graphene oxide-supported nanoscale zero-valent iron composites for the removal of atrazine from aqueous solution. Colloid. Surf. A 589, 124466. https://doi.org/10.1016/j.colsurfa.2020.124466.
- Xu, L., Campos, L.C., Li, J., Karu, K., Ciric, L., 2021. Removal of antibiotics in sand, GAC, GAC sandwich and anthracite/sand biofiltration systems. Chemosphere 275, 130004. https://doi.org/10.1016/j.chemosphere.2021.130004.
- Yan, C., Huang, J., Cao, C., 2021. Response of constructed wetland for wastewater treatment to graphene oxide: perspectives on plant and microbe. J. Hazard. Mater. 422, 126911 https://doi.org/10.1016/j.jhazmat.2021.126911.

- Yin, X., Qiao, S., Yu, C., Tian, T., Zhou, J., 2015. Effects of reduced graphene oxide on the activities of anammox biomass and key enzymes. Chem. Eng. J. 276, 106–112. https://doi.org/10.1016/j.cej.2015.04.073.
- Yousefi, M., Dadashpour, M., Mokhtarzadeh, A., 2017. Anti-bacterial activity of graphene oxide as a new weapon nanomaterial to combat multidrug-resistance bacteria. Mater. Sci. Eng. C 74, 568–581. https://doi.org/10.1016/j. msec.2016.12.125.
- Yuan, J., Passeport, E., Hofmann, R., 2022. Understanding adsorption and biodegradation in granular activated carbon for drinking water treatment: a critical review. Water Res. 210 (December 2021), 118026 https://doi.org/10.1016/j. watres.2021.118026.
- Zearley, T.L., Summers, R.S., 2012. Removal of trace organic micropollutants by drinking water biological filters. Environ. Sci. Technol. 46 (17), 9412–9419. https://doi.org/ 10.1021/es301428e.
- Zhang, S., Courtois, S., Axe, L., 2018a. Microbial community analysis in biologically active filters exhibiting efficient removal of emerging contaminants and impact of operational conditions. Sci. Total Environ. 1455–1464. https://doi.org/10.1016/j.scitotenv.2018.06.027, 640-641.
- Zhang, S., Gitungo, S., Axe, L., 2016. A pilot plant study using conventional and advanced water treatment processes: evaluating removal efficiency of indicator compounds representative of pharmaceuticals and personal care products. Water Res. 105, 85–96. https://doi.org/10.1016/j.watres.2016.08.033.
- Zhang, S., Gitungo, S.W., Axe, L., 2017. Biologically active filters An advanced water treatment process for contaminants of emerging concern. Water Res. 114, 31–41. https://doi.org/10.1016/j.watres.2017.02.014.

- Zhang, S., Wang, H., Liu, J., Bao, C., 2020. Measuring the specific surface area of monolayer graphene oxide in water. Mater. Lett. 261, 127098 https://doi.org/ 10.1016/j.matlet.2019.127098.
- Zhang, T., Tremblay, P.-L., 2020. Graphene: an antibacterial agent or a promoter of bacterial proliferation? iScience 23 (12), 101787. https://doi.org/10.1016/j. isci.2020.101787.
- Zhang, Y., Cao, B., Zhao, L., Sun, L., 2018b. Biochar-supported reduced graphene oxide composite for adsorption and coadsorption of atrazine and lead ions. Appl. Surf. Sci. 427, 147–155. https://doi.org/10.1016/j.apsusc.2017.07.237.
- Zhang, Z., Schniepp, H.C., Adamson, D.H., 2019. Characterization of graphene oxide: variations in reported approaches. Carbon N Y 154, 510–521. https://doi.org/ 10.1016/j.carbon.2019.07.103.
- Zhang, Z., Wang, L., Ji, Y., Cao, R., Zhou, J., Li, M., Zhu, L., Xu, X., 2023. Understanding the N-acylated homoserine lactones(AHLs)-based quorum sensing for the stability of aerobic granular sludge in the aspect of substrate hydrolysis enhancement. Sci. Total Environ. 858 (866), 159581 https://doi.org/10.1016/j.scitotenv.2022.159581.
- Zhou, H., Xu, G., 2020. Biofilm characteristics, microbial community structure and function of an up-flow anaerobic filter-biological aerated filter (UAF-BAF) driven by COD/N ratio. Sci. Total Environ. 708, 134422 https://doi.org/10.1016/j. scitotenv.2019.134422.
- Zhou, Y., Apul, O.G., Karanfil, T., 2015. Adsorption of halogenated aliphatic contaminants by graphene nanomaterials. Water Res. 79, 57–67. https://doi.org/ 10.1016/j.watres.2015.04.017.
- Zou, X., Zhang, L., Wang, Z., Luo, Y., 2016. Mechanisms of the antimicrobial activities of graphene materials. J. Am. Chem. Soc. 138 (7), 2064–2077. https://doi.org/ 10.1021/jacs.5b11411.